micromachines

Article

Tunable Electromechanical Coupling Coefficient of a Laterally Excited Bulk Wave Resonator with Composite Piezoelectric Film

Ying Xie [1], Yan Liu [1], Jieyu Liu [1], Lei Wang [1], Wenjuan Liu [1,2], Bo Woon Soon [3], Yao Cai [1,2,*] and Chengliang Sun [1,2,*]

[1] The Institute of Technological Sciences, Wuhan University, Wuhan 430072, China; _xieying@whu.edu.cn (Y.X.); liuyan92@whu.edu.cn (Y.L.); jieyuuu@whu.edu.cn (J.L.); lei_wang@whu.edu.cn (L.W.); lwjwhu@whu.edu.cn (W.L.)
[2] Hubei Yangtze Memory Laboratories, Wuhan 430205, China
[3] School of Microelectronics, Wuhan University, Wuhan 430072, China; soonbowoon@gmail.com
* Correspondence: caiyao999@whu.edu.cn (Y.C.); sunc@whu.edu.cn (C.S.)

Abstract: A resonator with an appropriate electromechanical coupling coefficient (K_t^2) is crucial for filter applications in radio communication. In this paper, we present an effective method to tune the K_t^2 of resonators by introducing different materials into a lithium niobate ($LiNbO_3$) piezoelectric matrix. The effective piezoelectric coefficients e_{33}^{eff} and e_{15}^{eff} of composite materials with four different introduced materials were calculated. The results show that the e_{15}^{eff} of $SiO_2/LiNbO_3$ composite piezoelectric material was mostly sensitive to an increase in the width of introduced SiO_2 material. Simultaneously, the simulation of a laterally excited bulk wave resonator (XBAR) with $SiO_2/LiNbO_3$ composite material was also carried out to verify the change in the K_t^2 originating from the variation in e_{15}^{eff}. The achievable n79 filter using the $SiO_2/LiNbO_3$ composite material demonstrates the promising prospects of tuning K_t^2 by introducing different materials into a $LiNbO_3$ piezoelectric matrix.

Keywords: composite piezoelectric material; electromechanical coupling coefficient K_t^2; laterally excited bulk wave resonator (XBAR); filter

Citation: Xie, Y.; Liu, Y.; Liu, J.; Wang, L.; Liu, W.; Soon, B.W.; Cai, Y.; Sun, C. Tunable Electromechanical Coupling Coefficient of a Laterally Excited Bulk Wave Resonator with Composite Piezoelectric Film. *Micromachines* **2022**, *13*, 641. https://doi.org/10.3390/mi13040641

Academic Editor: Giancarlo C. Righini

Received: 23 March 2022
Accepted: 15 April 2022
Published: 18 April 2022

1. Introduction

To balance the needs of wide-area coverage and high data rates, 5G new radio (NR) has been proposed [1,2]. Laterally excited bulk acoustic wave resonators (XBAR) are promising candidates for application in fifth-generation mobile communication due to their high frequency, large electromechanical coupling coefficient (K_t^2), low cost and complementary metal oxide semiconductor (CMOS) compatibility [3–7]. Victor Plessky realized a XBAR based on Z-cut lithium niobate ($LiNbO_3$) thin plate with a resonance frequency of approximately 4.9 GHz [8]. Ruochen Lu presented first-order antisymmetric (A1) mode resonators in thin 128° Y-cut $LiNbO_3$ films with a K_t^2 of 46.4% [9]. Bohua Peng designed and fabricated a solid-mounted-type XBAR on ZY-$LiNbO_3$, operating at 5 GHz [5]. The K_t^2 of XBAR has a significant influence on the bandwidth of filters. However, delicate control of the K_t^2 of XBARs is crucial for designing filters; for example, the K_t^2 of $LiNbO_3$-based XBARs is too large for specific n79 filters (4.4 GHz–5.0 GHz) [10].

The K_t^2 of XBAR can be adjusted by structural optimization and tuning the piezoelectric coefficients. Gianluca Piazza found that the K_t^2 can be tuned by changing the electrical boundary conditions imposed by the excitation electrodes, obtaining a range varying from 3% to 7% [11]. Jie Zou investigated the influence of the Euler angle and thickness of $LiNbO_3$ film on the K_t^2 of the resonator. It was found that the K_t^2 of the A1 mode acoustic wave varied rapidly with changes in the Euler angle [12]. V. Plessky analyzed the influence of pitch and duty factor on frequency and K_t^2 [13]. Using piezoelectric composite materials is another feasible method for K_t^2 tuning. In our previous work, we adopted a ScAlN/AlN composite piezoelectric film to achieve a Lamé Mode resonator with a high K_t^2 of 7.83% [14].

In this paper, we propose an effective method for tuning the K_t^2 of XBARs by applying composite film consisting of $LiNbO_3$ piezoelectric material and other materials. The tuning range was as high as 62%, which is efficient compared with other studies, as shown in Table 1. We used FEM to analyze the effective piezoelectric coefficients e_{33}^{eff} and e_{15}^{eff} of composite piezoelectric films with different volume fractions of different materials embedded in $LiNbO_3$ piezoelectric material. FEM simulative analysis of XBAR utilizing those composite piezoelectric films was also carried out. Finally, an n79 filter was designed using $SiO_2/LiNbO_3$ composite thin film-based XBARs with an adjustable K_t^2. The proposed XBAR with $LiNbO_3$-based composite piezoelectric film shows promising prospects for constructing filters with different bandwidths at high frequency.

Table 1. Comparison of the tuning effectiveness between our work and previous works.

Ref.	Method	K_t^2 (%)	Frequency	Tuning Effect
[12]	Change electrical boundary conditions	19%	484 MHz	10% to 19%
[13]	Change the Euler angle of $LiNbO_3$	55%	3.3 GHz	0% to 55%
[14]	Tuning structural parameters	25%	5 GHz	23% to 25%
This work	Composite piezoelectric material	32%	6 GHz	12% to 32%

2. Theoretical Calculation of Piezoelectric Coefficient

The theory of linear piezoelectricity couples the interaction between the electric and elastic variables via the following constitutive equations [15]:

$$\sigma_{ij} = C_{ijkl}\varepsilon_{kl} - e_{lij}E_i \tag{1}$$

$$D_i = e_{ikl}\varepsilon_{kl} + \kappa_{ik}E_k \tag{2}$$

where ε_{kl} and σ_{ij} are the components of the elastic strain and the components of the stress tensor, respectively; E_i and D_i are the components of the electric field and the components of the electric displacement, respectively; C_{ijkl} is the components of the fourth-order elastic stiffness tensor obtained in the absence of an applied electric field; e_{lij} is the components of the piezoelectric modulus tensor obtained without an applied strain; and κ_{ik} is the components of the dielectric modulus obtained without an applied strain.

It is convenient to treat the elastic and the electric variables in a similar fashion when modeling the piezoelectric behavior. This is accomplished by employing a notation introduced by Barnett and Lothe [16] and a generalized Voigt two-index notation [17]. Therefore, the constitutive equations can be represented as:

$$\begin{bmatrix} \sigma \\ D \end{bmatrix} = \begin{bmatrix} C & e^T \\ e & -\kappa \end{bmatrix} \begin{bmatrix} \varepsilon \\ -E \end{bmatrix} \tag{3}$$

The calculation of the effective properties of composite films is then realized utilizing the homogenization method, which relates the volume-averaged strain, stress, electric field, and electric displacement to the effective properties of the composite film. The composite films can thus be modeled as homogenized media. Using FEM, volume averages can be calculated as follows [18]:

$$\overline{\sigma_{ij}} = \frac{1}{V}S\sigma_{ij}dV = \frac{1}{V}\sum_{n=1}^{nel}\sigma_{ij}^{(n)}V^{(n)} \tag{4}$$

$$\overline{\varepsilon_{ij}} = \frac{1}{V}S\varepsilon_{ij}dV = \frac{1}{V}\sum_{n=1}^{nel}\varepsilon_{ij}^{(n)}V^{(n)} \tag{5}$$

$$\overline{D_i} = \frac{1}{V}SD_idV = \frac{1}{V}\sum_{n=1}^{nel}D_i^{(n)}V^{(n)} \tag{6}$$

$$\overline{E_i} = \frac{1}{V}SE_i dV = \frac{1}{V}\sum_{n=1}^{nel} E_i^{(n)} V^{(n)} \tag{7}$$

where V is the volume of the representative volume elements (RVE). $\overline{\sigma_{ij}}$, $\overline{\varepsilon_{ij}}$, $\overline{D_i}$, and $\overline{E_i}$ are the volume-averaged values of stress, strain, electric displacement, and electric field, respectively.

In terms of these average values, the constitutive equations of linear piezoelectricity for composite material can be expressed in matrix form as follows:

$$\begin{Bmatrix} \overline{\sigma_{11}} \\ \overline{\sigma_{22}} \\ \overline{\sigma_{33}} \\ \overline{\sigma_{23}} \\ \overline{\sigma_{13}} \\ \overline{\sigma_{12}} \\ \overline{D_1} \\ \overline{D_2} \\ \overline{D_3} \end{Bmatrix} = \begin{bmatrix} C_{11}^{eff} & C_{12}^{eff} & C_{13}^{eff} & C_{14}^{eff} & 0 & 0 & 0 & -e_{22}^{eff} & e_{31}^{eff} \\ C_{12}^{eff} & C_{11}^{eff} & C_{13}^{eff} & -C_{14}^{eff} & 0 & 0 & 0 & e_{22}^{eff} & e_{31}^{eff} \\ C_{13}^{eff} & C_{13}^{eff} & C_{33}^{eff} & 0 & 0 & 0 & 0 & 0 & e_{33}^{eff} \\ C_{14}^{eff} & -C_{14}^{eff} & 0 & C_{44}^{eff} & 0 & 0 & 0 & e_{15}^{eff} & 0 \\ 0 & 0 & 0 & 0 & C_{44}^{eff} & C_{14}^{eff} & e_{15}^{eff} & 0 & 0 \\ 0 & 0 & 0 & 0 & C_{14}^{eff} & C_{66}^{eff} & e_{22}^{eff} & 0 & 0 \\ 0 & 0 & 0 & 0 & e_{15}^{eff} & e_{22}^{eff} & -\kappa_{11}^{eff} & 0 & 0 \\ -e_{22}^{eff} & e_{22}^{eff} & 0 & e_{15}^{eff} & 0 & 0 & 0 & -\kappa_{11}^{eff} & 0 \\ e_{31}^{eff} & e_{31}^{eff} & e_{33}^{eff} & 0 & 0 & 0 & 0 & 0 & -\kappa_{33}^{eff} \end{bmatrix} \begin{Bmatrix} \overline{\varepsilon_{11}} \\ \overline{\varepsilon_{22}} \\ \overline{\varepsilon_{33}} \\ 2\overline{\varepsilon_{23}} \\ 2\overline{\varepsilon_{13}} \\ 2\overline{\varepsilon_{12}} \\ -\overline{E_1} \\ -\overline{E_2} \\ -\overline{E_3} \end{Bmatrix} \tag{8}$$

As shown in Figure 1, the RVE consisted of Z-cut $LiNbO_3$ and other materials. Other materials were embedded in the thin $LiNbO_3$ film, and the width of the other materials is expressed as P. Here, four different materials commonly used in MEMS were taken under consideration, including SiC, Al_2O_3, AlN and SiO_2. The boundary conditions applied to the six surfaces of the RVE are in the form of prescribed displacements and prescribed electric potentials. For calculation of the piezoelectric coefficients e_{33}^{eff} and e_{15}^{eff}, the boundary conditions applied to the six surfaces and the postprocessing steps for assessing the piezoelectric coefficients e_{33}^{eff} and e_{15}^{eff} are listed in Table 2. In Table 2, u, v, and w are the displacement components along the x-, y-, and z-coordinate axes, respectively, and $V0$ is the applied electric potential.

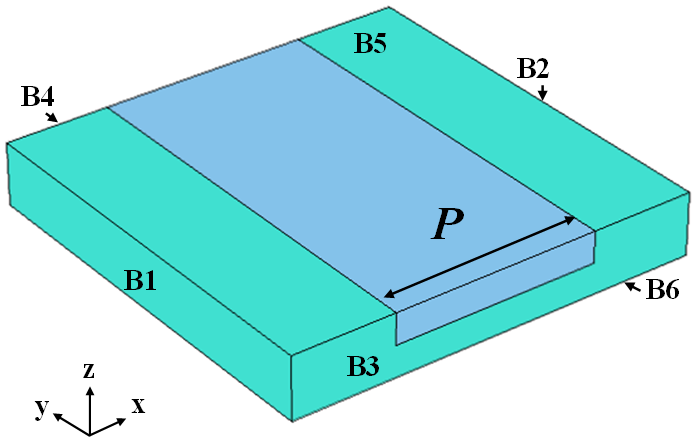

Figure 1. Images of full representative volume elements (RVEs). The green regions represent the LiNbO3 material, whereas the blue region represents the other material.

Table 2. Boundary conditions for evaluating the effective properties of the composite.

Effective Property	B1	B2	B3	B4	B5	B6	Formula
e_{15}^{eff}	$u = 0$	$u = 0$	$v = 0$ $\varphi = 0$	$v = 0$ $\varphi = V0$	$w = 0$	$w = 0$	$e_{15}^{eff} = -\frac{\overline{\sigma}_{23}}{\overline{E}_2}$
e_{33}^{eff}	$u = 0$	$u = 0$	$v = 0$	$v = 0$	$w = 0$ $\varphi = 0$	$w = 0$ $\varphi = V0$	$e_{33}^{eff} = -\frac{\overline{\sigma}_{33}}{\overline{E}_3}$

The calculated effective piezoelectric coefficients e_{33}^{eff} and e_{15}^{eff} of $LiNbO_3$ composites using all four kinds of materials are presented as a function of the width of material (P) in Figure 2. The P of the other material ranged from zero to a maximum of 19 µm. It is shown that the effective piezoelectric coefficients e_{33}^{eff} and e_{15}^{eff} declined predictably with an increase in P for all four kinds of $LiNbO_3$-based composite film. Among the four different composite materials, the effective piezoelectric coefficients e_{33}^{eff} and e_{15}^{eff} of the $SiO_2/LiNbO_3$ composite material had the largest variation. The e_{33}^{eff} of $AlN/LiNbO_3$ composite film changed the most gradually, while the e_{15}^{eff} of $SiC/LiNbO_3$ composite film had the smallest variation. The effective piezoelectric coefficient e_{15}^{eff} of $SiO_2/LiNbO_3$ composite material varied from 3.65 to 1.31 as P increased from 0 to 19 µm, for which the tuning range could reach as high as 64.1%.

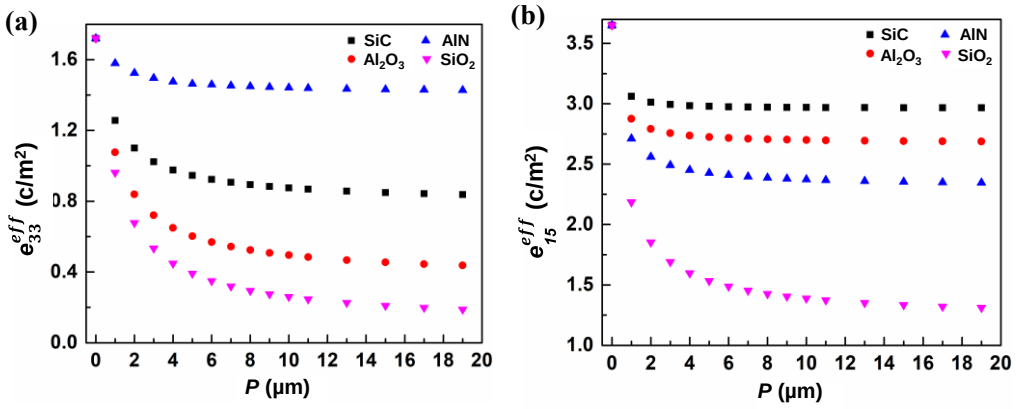

Figure 2. Effective piezoelectric coefficients e_{33}^{eff} (**a**) and e_{15}^{eff} (**b**) of four different $LiNbO_3$-based composite materials as function of the width of nonpiezoelectric materials (P).

3. FEM Simulation of XBAR

FEM simulation of an XBAR with $LiNbO_3$ composite material was also carried out to demonstrate tuning of the K_t^2. As illustrated in Figure 3a, the XBAR consisted of a suspended 300 nm-thick $LiNbO_3$ composite platelet and a set of 100 nm-thick Mo electrodes on top. The electrical potentials were alternatingly applied to adjacent electrodes, as illustrated by the "+" and "−" signs in Figure 3b, creating a lateral electric field along the X axis. Due to the strong piezoelectric coefficient e_{15}^{eff} of $LiNbO_3$, the alternating lateral electric field could excite vertical shear vibration in A1 mode within the platelet [19]. Structural optimization was implemented by adjusting the P of the SiO_2 embedded in the thin $LiNbO_3$ film within a range from 0 to 15 µm, while the thickness of SiO_2 (t) remained 150 nm, as shown in Figure 3c.

The series frequency of XBAR with thin $LiNbO_3$ film ($p = 0$) is approximately 6.14 GHz and the parallel frequency is 7.25 GHz. As the value of p increased, the parallel frequency of XBAR declined consistently, while the series frequency remained almost the same, as shown in Figure 4. The parallel frequency declined from 7.25 GHz to 6.52 GHz as P increased from 0 to 15 µm. The series frequency of XBAR can be expressed as the following formula [20]:

$$f_s = \sqrt{\left(\frac{v_z}{2h}\right)^2 + \left(\frac{v_x}{2G}\right)^2} \quad (9)$$

where h is the thickness of the piezoelectric thin film and G is the gap between two adjacent electrodes. In our simulations, the thickness of the piezoelectric thin film and the gap between two adjacent electrodes remained the same; therefore, it is reasonable to

assume that the series frequency remained almost constant. The effective electromechanical coupling coefficient (K_t^2) can be calculated using the following formula [21,22]:

$$K_t^2 = \frac{K^2}{1+K^2} = \frac{\pi^2}{4} \times \frac{f_s}{f_p} \times \frac{(f_p - f_s)}{f_p} \tag{10}$$

$$K^2 = \frac{e_{15}^2}{\varepsilon_r \varepsilon_0 C_{44}} \tag{11}$$

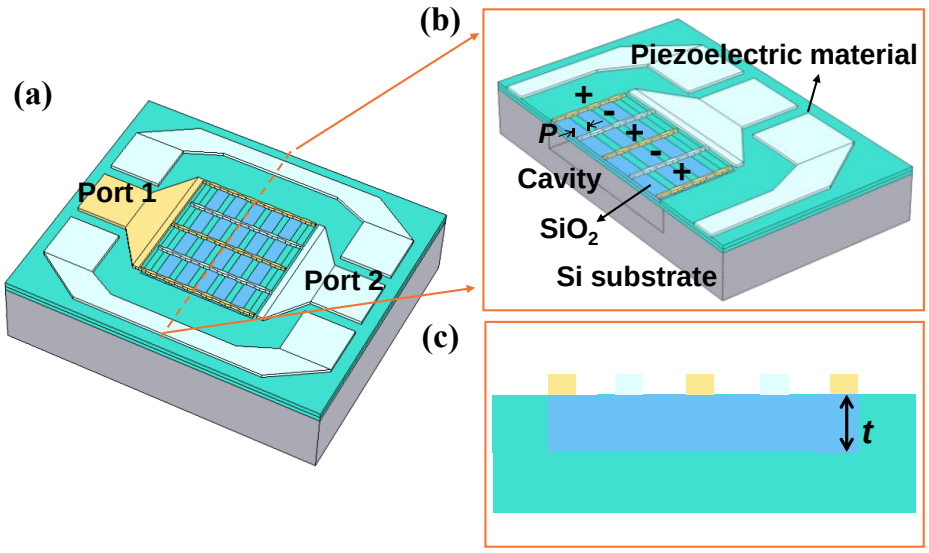

Figure 3. (**a**) Schematic drawing of laterally excited bulk acoustic wave resonator using composite piezoelectric material. (**b**) Sectional view of the resonator cut across the dashed line. (**c**) 2D schematic of the effective working area along the dashed line.

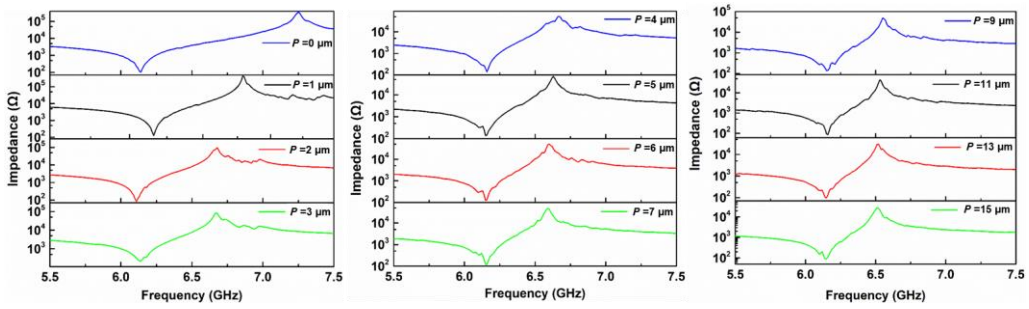

Figure 4. The impedance curves of XBARs with different widths of nonpiezoelectric materials (P) ranging from 0 to 15 μm.

As shown in Figure 5, when P increased to 1 μm, K_t^2 decreased sharply from 32% to 20.7%, and K_t^2 then declined slowly with the increase in P from 2 to 11 μm. When P increased beyond 11 μm, K_t^2 no longer changed. The variation trend of K_t^2 is highly consistent with the change in the calculated effective piezoelectric coefficient e_{15}^{eff}, which demonstrates that introducing other materials to a $LiNbO_3$ piezoelectric matrix is an effective method for tuning the K_t^2 of XBARs.

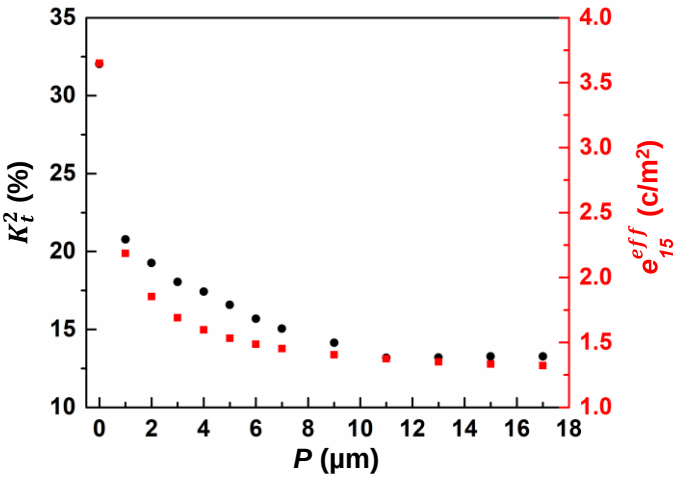

Figure 5. The variation in K_t^2 and e_{15}^{eff} with different widths (P) of nonpiezoelectric materials.

Here, we provide a possible fabrication process flow for our devices, as shown in Figure 6. The substrate wafer consists of a thin Z-cut $LiNbO_3$ film and a Si substrate. Firstly, the thin $LiNbO_3$ film is etched via electron beam lithography; the depth is controlled by the etching time. A 150 nm-thick layer of SiO_2 is deposited on the surface of the $LiNbO_3$ film and then polished to a smooth plate. Then, molybdenum (Mo) electrodes are deposited on the surface of the thin $SiO_2/LiNbO_3$ film and patterned by lithography and reactive ion etching technology. Subsequently, the release holes are realized via electron beam lithography, which enables formation of the cavity by removing the Si substrate with Xef_2. By exactly controlling the release time, resonators with only a suspended working area are realized.

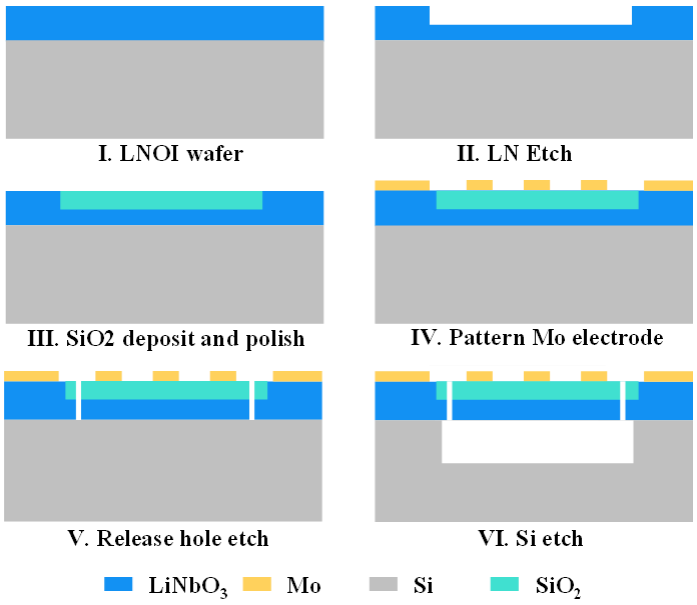

Figure 6. The fabrication process flow for the proposed devices.

4. Design of N79 Filters

As discussed in Section 3, the K_t^2 of XBAR can be adjusted by introducing other materials into the $LiNbO_3$ piezoelectric film, which enables the construction of different bandwidth filters for 5G. For example, the K_t^2 of an XBAR based on pure $LiNbO_3$ film is calculated as being approximately 35% and the −3 dB bandwidth of the corresponding filter is 1050 MHz, as shown in Figure 7a,c, which exceeds the bandwidth requirements of the n79 filter. As seen from Figure 5, the K_t^2 of XBARs decreased to approximately 21%

when the P of the SiO_2 in the $SiO_2/LiNbO_3$ composite film was 1 μm, which is suitable for the bandwidth requirement of the n79 filter. Therefore, we designed a filter based on thin $SiO_2/LiNbO_3$ composite film with a P of 1 μm. The resonant and anti-resonant frequencies of the series resonator were 4.71 GHz and 5.17 GHz, respectively, and those of the parallel resonator were 4.35 GHz and 4.7 GHz, respectively, as shown in Figure 7b. As shown in Figure 7d, the transmission response of the filter showed a −3 dB bandwidth of 600 MHz, ranging from 4.4 GHz to 5.0 GHz, which satisfies the requirements of the n79 very well.

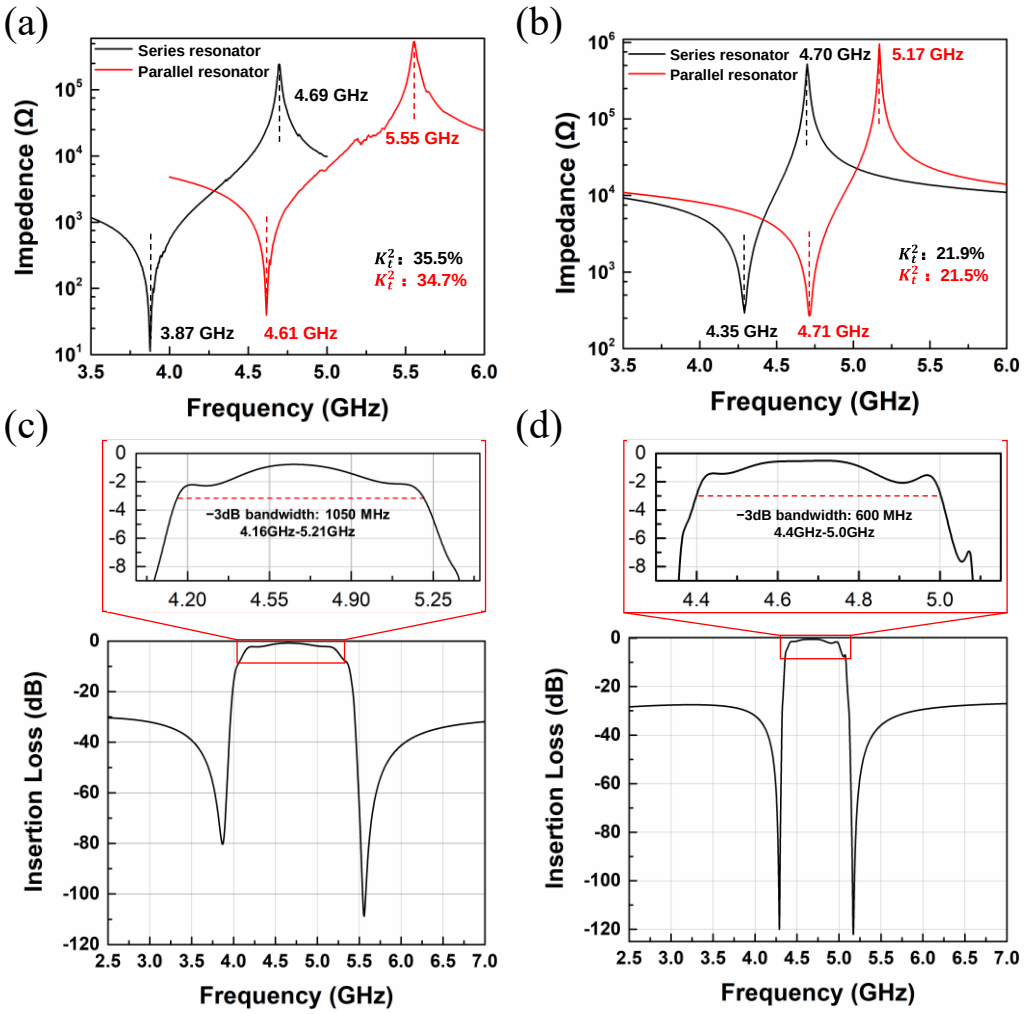

Figure 7. (**a**) The impedance curves of an XBAR with pure $LiNbO_3$ film for the n79 filter. (**b**) The impedance curves of an XBAR with $SiO_2/LiNbO_3$ composite film for the n79 filter. (**c**) The response of the proposed filter with pure $LiNbO_3$ film. (**d**) The response of the proposed filter with $SiO_2/LiNbO_3$ composite film.

5. Conclusions

In summary, an effective method for tuning the K_t^2 of XBARs, by using composite piezoelectric materials combining $LiNbO_3$ piezoelectric material with other materials, is demonstrated in this work. The effective piezoelectric coefficients e_{33}^{eff} and e_{15}^{eff} of the four kinds of $LiNbO_3$-based composite materials were calculated through FEM simulation. Among the four different composite materials, the effective piezoelectric coefficients e_{33}^{eff} and e_{15}^{eff} of the $SiO_2/LiNbO_3$ composite material had the largest variation. The e_{15}^{eff} of $SiO_2/LiNbO_3$ composite material declined from 3.65 to 1.31 as P increased from 0 to 19 μm. The e_{33}^{eff} of $SiO_2/LiNbO_3$ composite material declined from 1.72 to 0.19 as P increased from 0 to 19 μm. Simultaneously, we also carried out the simulation of an XBAR using

$SiO_2/LiNbO_3$ composite material to verify the change in the K_t^2, owing to the variation in e_{15}^{eff}. The K_t^2 decreased from 34% to approximately 11% as P increased from 0 to 17 μm, which was highly consistent with the change in e_{15}^{eff}. Finally, we designed a filter made with $SiO_2/LiNbO_3$ composite material, which satisfied the bandwidth requirement of the n79 very well, demonstrating that XBARs with $LiNbO_3$-based composite piezoelectric film show fascinating prospects for fabricating different bandwidth filters at high frequencies in the future.

Author Contributions: Conceptualization, Y.X.; Formal analysis, Y.L.; Investigation, Y.X.; Methodology, L.W., Y.C. and C.S.; Writing—original draft, Y.X.; Writing—review & editing, J.L., W.L., B.W.S., Y.C. and C.S. All authors have read and agreed to the published version of the manuscript.

Funding: This work was supported by the National Key R&D Program of China (No. 2020YFB2008803).

Conflicts of Interest: The authors declare no conflict of interest.

References

1. Ruppel, C.C.W. Acoustic Wave Filter Technology–A Review. *IEEE Trans. Ultrason. Ferroelectr. Freq. Control.* **2017**, *64*, 1390–1400. [CrossRef] [PubMed]
2. Takai, T.; Iwamoto, H.; Takamine, Y.; Nakao, T.; Hiramoto, M.; Koshino, M.I.H.P. SAW technology and its application to micro acoustic components. In Proceedings of the 2017 IEEE International Ultrasonics Symposium (IUS), Washington, DC, USA, 6–9 September 2017; p. 1.
3. Koskela, J.; Plessky, V.P.; Willemsen, B.A.; Turner, P.J.; Garcia, B.; Hammond, R.B.; Fenzi, N.O. Fast GPU-Assisted FEM Simulations of 3D Periodic TCSAW, IHP, and XBAR Devices. In Proceedings of the 2019 IEEE International Ultrasonics Symposium (IUS), Scotland, UK, 6–9 October 2019; pp. 181–184.
4. Koulakis, J.; Koskela, J.; Yang, W.; Myers, L.; Dyer, G.; Garcia, B. XBAR physics and next generation filter design. In Proceedings of the 2021 IEEE International Ultrasonics Symposium (IUS), Xi'an, China, 11–16 September 2021; pp. 1–5.
5. Peng, B.; Hu, N.; Jia, B.; Wang, H. A novel N79 filter using solid-mounted A1-mode resonator for 5G applications. In Proceedings of the 2021 IEEE International Ultrasonics Symposium (IUS), Xi'an, China, 11–16 September 2021; pp. 1–4.
6. Yang, Y.; Gao, A.; Lu, R.; Gong, S. 5 Ghz lithium niobate MEMS resonators with high FoM of 153. In Proceedings of the 2017 IEEE 30th International Conference on Micro Electro Mechanical Systems (MEMS), Las Vegas, NV, USA, 22–26 January 2017; pp. 942–945.
7. Gong, S.; Piazza, G. Laterally vibrating lithium niobate MEMS resonators with high electromechanical coupling and Quality factor. In Proceedings of the 2012 IEEE International Ultrasonics Symposium, Dresden, Germany, 7–10 October 2012; pp. 1051–1054.
8. Plessky, V.; Yandrapalli, S.; Turner, P.J.; Villanueva, L.G.; Koskela, J.; Faizan, M.; Pastina, A.D.; Garcia, B.; Costa, J.; Hammond, R.B. Laterally excited bulk wave resonators (XBARs) based on thin Lithium Niobate platelet for 5GHz and 13 GHz filters. In Proceedings of the 2019 IEEE MTT-S International Microwave Symposium (IMS), Boston, MA, USA, 2–7 June 2019; pp. 512–515.
9. Lu, R.; Yang, Y.; Link, S.; Gong, S. A1 Resonators in 128° Y-cut Lithium Niobate with Electromechanical Coupling of 46.4%. *J. Microelectromech. Syst.* **2020**, *29*, 313–319. [CrossRef]
10. Faizan, M.; Pastina, A.D.; Yandrapalli, S.; Turner, P.J.; Hammond, R.B.; Plessky, V.; Villanueva, L.G. Fabrication Of Lithium Niobate Bulk Acoustic Resonator For 5G Filters. In Proceedings of the 2019 20th International Conference on Solid-State Sensors, Actuators and Microsystems & Eurosensors XXXIII (TRANSDUCERS & EUROSENSORS XXXIII), Berlin, Germany, 23–27 June 2019; pp. 1752–1755.
11. Gong, S.; Piazza, G. Large frequency tuning of Lithium Niobate laterally vibrating MEMS resonators via electric boundary reconfiguration. In Proceedings of the 2013 Transducers & Eurosensors XXVII: The 17th International Conference on Solid-State Sensors, Actuators and Microsystems (TRANSDUCERS & EUROSENSORS XXVII), Barcelona, Spain, 16–20 June 2013; pp. 2465–2468.
12. Zou, J.; Yantchev, V.; Iliev, F.; Plessky, V.; Samadian, S.; Hammond, R.B.; Turner, P.J. Ultra-Large-Coupling and Spurious-Free SH_0 Plate Acoustic Wave Resonators Based on Thin $LiNbO_3$. *IEEE Trans. Ultrason. Ferroelectr. Freq. Control.* **2020**, *67*, 374–386. [CrossRef] [PubMed]
13. Yandrapalli, S.; Eroglu, S.E.K.; Plessky, V.; Atakan, H.B.; Villanueva, L.G. Study of Thin Film $LiNbO_3$ Laterally Excited Bulk Acoustic Resonators. *J. Microelectromech. Syst.* **2022**, *31*, 217–225. [CrossRef]
14. Zhou, J.; Liu, Y.; Xu, Q.; Xie, Y.; Cai, Y.; Liu, J.; Liu, W.; Tovstopyat, A.; Sun, C. ScAlN/AlN Film-Based Lamé Mode Resonator With High Effective Electromechanical Coupling Coefficient. *J. Microelectromech. Syst.* **2021**, *30*, 677–679. [CrossRef]
15. Piazza, G.; Stephanou, P.J.; Pisano, A.P. Single-Chip Multiple-Frequency ALN MEMS Filters Based on Contour-Mode Piezoelectric Resonators. *J. Microelectromech. Syst.* **2007**, *16*, 319–328. [CrossRef]
16. Barnett, D.M.; Lothe, J. Dislocations and line charges in anisotropic piezoelectric insulators. *Phys. Status Solidi* **1975**, *67*, 105–111. [CrossRef]

17. Dunn, M.L.; Taya, M. Micromechanics predictions of the effective electroelastic moduli of piezoelectric composites. *Int. J. Solids Struct.* **1993**, *30*, 161–175. [CrossRef]
18. Mishra, N.; Krishna, B.; Singh, R.; Das, K. Evaluation of Effective Elastic, Piezoelectric, and Dielectric Properties of SU8/ZnO Nanocomposite for Vertically Integrated Nanogenerators Using Finite Element Method. *J. Nanomater.* **2017**, *2017*, 1–14. [CrossRef]
19. Yandrapalli, S.; Plessky, V.; Koskela, J.; Yantchev, V.; Turner, P.; Villanueva, L.G. Analysis of XBAR resonance and higher order spurious modes. In Proceedings of the 2019 IEEE International Ultrasonics Symposium (IUS), Scotland, UK, 6–9 October 2019; pp. 185–188.
20. Yang, Y.; Lu, R.; Manzaneque, T.; Gong, S. Toward Ka Band Acoustics: Lithium Niobate Asymmetrical Mode Piezoelectric MEMS Resonators. In Proceedings of the 2018 IEEE International Frequency Control Symposium (IFCS), Olympic Valley, CA, USA, 21–24 May 2018; pp. 1–5.
21. Lu, R.; Li, M.H.; Yang, Y.; Manzaneque, T.; Gong, S. Accurate Extraction of Large Electromechanical Coupling in Piezoelectric MEMS Resonators. *J. Microelectromech. Syst.* **2019**, *28*, 209–218. [CrossRef]
22. Zhang, Y.; Wang, L.; Zou, Y.; Xu, Q.; Liu, J.; Wang, Q.; Tovstopyat, A.; Liu, W.; Sun, C.; Yu, H. Lithium Niobate Thin Film Based A3 Mode Resonators with High Effective Coupling Coefficient of 6.72%. In Proceedings of the 2021 IEEE 34th International Conference on Micro Electro Mechanical Systems (MEMS), Gainesville, FL, USA, 25–29 January 2021; pp. 466–469.